Journal of Catalysis 280 (2011) 28–39

Contents lists available at ScienceDirect

Journal of Catalysis

journal homepage: www.elsevier.com/locate/jcat

Oxidative dehydrogenation of ethane over Ni–W–O mixed metal oxide catalysts

B. Solsona [a], J.M. López Nieto [b,*], P. Concepción [b], A. Dejoz [a], F. Ivars [b], M.I. Vázquez [a]

[a] Dep. Ingeniería Química, Univ. Valencia, 46100 Burjassot, Spain
[b] Instituto de Tecnología Química (UPV-CSIC), Campus Universidad Politécnica de Valencia, Avenida de los Naranjos s/n, 46022 Valencia, Spain

ARTICLE INFO

Article history:
Received 28 December 2010
Revised 23 February 2011
Accepted 24 February 2011
Available online 13 April 2011

Keywords:
Nickel tungsten metal oxide catalysts
Oxidative dehydrogenation of ethane
Ethylene oxidation
Catalyst characterization
XPS
TPR
XRD
Raman
FTIR of adsorbed CO
Oxygen isotopic exchange

ABSTRACT

Ni–W–O mixed oxides were prepared through the evaporation of aqueous solutions of nickel nitrate and ammonium tungstate and calcined in air at 500 °C for 2 h. The catalysts were characterized by several techniques (N_2 adsorption, X-ray diffraction, temperature-programmed reduction, X-ray photoelectron spectroscopy, Fourier transform infrared spectroscopy of adsorbed CO, and $^{18}O/^{16}O$ isotope exchange) and tested in the oxidative dehydrogenation of ethane. The catalytic activity and catalyst reducibility decrease when the W content increases. Thus, nickel sites seem to be the active centers for ethane activation in these catalysts. However, the selectivity to ethylene strongly changes depending on the Ni/W ratio. In W-rich catalysts, in which $NiWO_4$ and WO_3 are mainly observed, a strong influence of ethane conversion on the selectivity to ethylene is observed. However, in Ni-rich catalysts, in which NiO crystallites and WO_x nanoparticles are mainly observed, ethane conversion hardly influences the selectivity to ethylene. It has been demonstrated that the nature of the Ni sites and the characteristics and number of the acid sites determine the catalytic behavior of these catalysts. The presence of Lewis acid sites with high acid strength in W-rich catalysts facilitates the decomposition of ethylene during ethane oxidation.

1. Introduction

Ethylene is the principal petrochemical building block and is a major feedstock for polymers. Global ethylene production capacity as of January 2009 was 126.7 million tons per year [1], and it is expected to increase significantly in the near future. However, ethylene is currently produced in addition to propylene by steam cracking of hydrocarbons, the most energy-consuming process in the chemical industry [2]. Oxidative dehydrogenation of lower alkanes is an interesting alternative to the current industrial processes (steam cracking or catalytic dehydrogenation) for the production of olefins [3–6]. In fact, ethylene could be produced by the oxidative dehydrogenation of ethane (ODHE), an exothermic process operating at about 400 °C in which catalyst deactivation by coke can be minimized because of the presence of molecular oxygen as an oxidant in the reactor feed. However, the development of both active and selective catalytic materials proves to be a very hard task, since the desired products, olefins, are usually more reactive than the corresponding alkanes, so that the formation of carbon oxides is the thermodynamically favored route [3–6].

From an industrial point of view, it has been proposed that ethylene yields between 65% and 70% are required to compete with the steam-cracking process [3,6]. Several catalytic systems have been proposed in the past two decades, and it is known that the reaction conditions and the mechanism involved strongly depend on the catalytic system [2–7]. At the moment, the limiting factor in the development of most of the proposed catalytic systems is the high formation of carbon oxides, especially by the consecutive deep oxidation of ethylene [2–7]. This has been improved by using MoVTeNbO catalysts, which seems to be the most competitive alternative nowadays to the current industrial process in ethylene production [8,9]. However, the ethylene productivity achieved with these catalysts is probably still low for their industrial implementation.

NiO-based mixed oxides are also potential catalysts for ODHE [18–21], especially Ni–Nb–O materials [11–14]. Nickel is a low-cost metal capable of activating ethane at very low temperatures. The incorporation of niobium makes this catalyst more selective. A drastic decrease in surface area has been observed after catalytic tests, but it only causes a small decrease in catalytic performance. After 100 h on line, the surface area of a Ni–Nb–O catalyst decreased 40%, while the ethane conversion only dropped from 42% to 38%, with the selectivity to ethylene remaining constant [18].

Recently, it has been reported that alumina-supported Ni–W–O mixed oxides are also active and relatively selective in ODHE [21]. As with Ni–Nb–O catalysts, one interesting feature of this catalytic system is that ethylene deep oxidation during the oxidative dehydrogenation of ethane can be minimized by controlling the catalyst composition.

* Corresponding author.
E-mail address: jmlopez@itq.upv.es (J.M. López Nieto).

0021-9517/$ - see front matter © 2011 Elsevier Inc. All rights reserved.
doi:10.1016/j.jcat.2011.02.010

The goal of this work is the synthesis, characterization, and investigation of the catalytic behavior of bulk Ni–W–O mixed oxides in the ODHE. It will be shown that the variation of the selectivity to ethylene with ethane conversion and the physicochemical properties (using appropriate characterization techniques) depend strongly on the catalyst composition. In addition, it will be shown that both primary and consecutive nonselective steps in this reaction can be tuned by changing the Ni/W ratio in the catalysts.

2. Experimental

2.1. Catalyst preparation

Ni–W–O mixed metal oxide catalysts were prepared through the evaporation at 90 °C of aqueous solutions of nickel nitrate and ammonium tungstate. NiO and WO_3 were obtained by evaporation of the corresponding aqueous solutions at 90 °C. The solids were dried overnight in a furnace at 120 °C and finally calcined in static air for 2 h at 500 °C. The catalysts will be named NiW*n*, in which *n* corresponds to the atomic ratio W/(Ni + W).

The $NiWO_4$ single phase was prepared similarly to the other Ni–W–O catalysts by calcining the samples twice, first at 500 °C and later at 600 °C. The composition observed was that corresponding to $NiWO_4$, i.e., presenting a Ni/W atomic ratio of 1.

2.2. Catalyst characterization

Catalyst surface areas were determined by multipoint N_2 adsorption at −196 °C using the BET method.

Powder X-ray diffraction (XRD) was used to identify the crystalline phases present in the catalysts. An Enraf Nonius FR590 sealed tube diffractometer with a monochromatic Cu Kα_1 source operating at 40 kV and 30 mA was used.

Temperature-programmed reduction (TPR) was carried out in a Micromeritics Autochem 2910 equipped with a TCD detector, in which the reducing gas was 10% H_2 in Ar (total flow rate 50 ml min^{-1}). The temperature range explored was from room temperature to 800 °C. The heating rate was maintained at 10 °C min^{-1}.

X-ray photoelectron spectroscopy (XPS) measurements were taken on a SPECS spectrometer with an MCD-9 detector and using a nonmonochromatic Al Kα (1486.6 eV) X-ray source. Spectra were recorded using analyzer pass energy of 50 V and an X-ray power of 200 W and under an operating pressure of 10^{-9} mbar. Spectra treatment was performed using the CASA software. Binding energies (BE) were referenced to O1*s* at 361.5 eV.

FTIR spectra were collected with a FTS-40A BioRad spectrometer equipped with a DTGS detector (4 cm^{-1} resolution, 32 scans). An IR cell allowing in situ treatment under controlled atmospheres and temperatures from −176 to 500 °C was connected to a vacuum system with a gas dosing facility. Self-supporting pellets (ca. 10 mg cm^{-2}) were prepared from the sample powders and treated at 250 °C in oxygen flow of 20 ml min^{-1} for 1.5 h, followed by evacuation at 10^{-4} mbar at the same temperature for 1 h. After activation, the samples were cooled to −176 °C under dynamic vacuum conditions, followed by CO dosing at increasing pressure (0.4–8.5 mbar). IR spectra were recorded after each dosing.

Oxygen isotopic-exchange experiments were conducted using a quartz microreactor coupled to a quadrupole mass spectrometer (Omnistar QMG 220 M1). Before each experiment, the catalyst was pretreated in 50% $^{16}O_2$/Ar flow (36 ml/min) at 450 °C for 2.5 h, followed by cooling to 150 °C in the same 10% $^{16}O_2$/Ar flow. Once 150 °C was attained, oxygen was replaced by argon (20 ml min^{-1}) and keep at that temperature for 1.5 h before being cooled to 25 °C. For the temperature-programmed isotopic-exchange experiments (TPIE), the catalyst (0.162 g) was subjected to a 10% $^{18}O_2$/Ar flow (22 ml min^{-1}), and the temperature was raised from 25 to 650 °C at a heating rate of 10 °C/min. The concentration profiles of the exit gas composition were obtained by acquiring the mass spectra signals relative to $^{16}O_2$ (m/e = 32), $^{16}O^{18}O$ (m/e = 34) and $^{18}O_2$ (m/e = 36). Blank run experiments were carried out using an empty reactor in order to check contributions of the gas-phase reactions and stability of the mass spectrometer.

2.3. Catalytic tests

The catalytic experiments were carried out at atmospheric pressure, in the temperature range 200–475 °C, mainly at 400–450 °C, using a fixed-bed quartz tubular reactor (i.d. 20 mm, length 400 mm). The feed consisted of a mixture of C_2H_6/O_2/He with molar ratio of 30/30/40. Several catalyst weights (from 0.05 to 5 g) and total flows (from 20 to 150 ml min^{-1}) were studied. Catalyst samples were introduced into the reactor diluted with silicon carbide in order to keep constant volume in the catalytic bed. Reactants and products were analyzed by gas chromatography using two packed columns: (i) molecular sieve 5 Å (2.5 m) and (ii) Porapak Q (3 m). Blank runs showed no conversion at a reaction temperature of 475 °C.

3. Results and discussion

3.1. Catalyst characterization

Table 1 lists the characteristics of catalysts. Chemical analysis of W and Ni is in good agreement with the nominal composition. On the other hand, it can be seen that both pure NiO and WO_3 present low surface areas (4 and 9 m^2 g^{-1}, respectively). However, mixed oxides show higher surface areas even in the case of the lowest W loadings. The sample with a W/(Ni + W) atomic ratio of 0.26 presents the highest surface area, ca. 57 m^2 g^{-1}. This enhanced surface area of mixed Ni–W–O catalysts is likely due to the presence of a W heteroatom that hinders the crystallization of NiO, preventing the formation of large particles.

XRD patterns of calcined samples are shown in Fig. 1, while the description of crystalline phases is summarized in Table 1. For comparison, the XRD patterns of pure $NiWO_4$, with the main diffraction peaks at 2θ = 31.0°, 54.7°, 65.9°, 36.6°, 41.8°, 19.4°, 24.0°, and 25.0° [JCPDS: 15-0755] (Fig. 1, pattern h) have also been included. A W-free sample presents diffraction peaks at 2θ = 37.3°, 43.3°, and 62.9°, characteristic of cubic NiO [JCPDS: 78-0643] (Fig. 1, pattern a), while an Ni-free sample (i.e., NiW1) presents main diffraction peaks at 2θ = 23.19°, 23.59°, 24.38°, and 34.14°, which correspond to the (0 0 2), (0 2 0), (2 0 0), and (2 2 0) crystallographic planes, respectively, of monoclinic WO_3 [JCPDS: 43-1035] (Fig. 1, pattern g). For mixed metal oxides, the XRD patterns suggest an important decrease in the crystal sizes of both NiO and WO_3 and the appearance of new crystalline phases.

In the Ni-rich region (i.e., W/(Ni + W) ratio lower than 0.4), NiO is formed over almost all the catalysts, although the appearance of new diffraction peaks can also be seen at 2θ = 14.4°, 25.1°, 28.9°, 32.7°, 47.1°, 53.6°, 56.0°, 57.7°, and 61.7°, whose intensities increase with the W content up to W/(Ni + W) ratios of 0.36. Similar diffraction peaks have also been observed when a stoichiometric mixture of $H_{26}N_6O_{41}W_{12}{\cdot}18H_2O$ and $Ni(NO_3)_2{\cdot}6H_2O$ (Ni/W molar ratio of 1) at 400 °C was treated in air, and it has been related to tungsten trioxide of low crystallinity [22].

On the other hand, no changes in the NiO lattice constants have been observed (Table 1), suggesting that W^{6+} ions are not incorporated into the lattice of the NiO crystals. However, a broadening of the diffraction peaks related to NiO is clearly observed in the XRD

Table 1
Characteristics of Ni–W–O mixed metal oxide catalysts.

Catalysts	W/(Ni + W) Atomic ratio[a]	S_{BET} ($m^2\ g^{-1}$)	Crystalline phases[b]	NiO lattice constant[c] (Å)	Apparent activation energy $E_{a\ ethylene}$[d] (kJ mol^{-1})
NiW0	0	3.8	NiO	4.180	106
NiW0.1	0.09	35.7	NiO + WO_x[e]	4.181 (1)	109
NiW0.2	0.16	37.9	NiO + WO_x[e]	4.183 (1)	96
NiW0.3	0.26	57.1	NiO + WO_x[e]	4.178 (2)	91
NiW0.36	0.33	50.7	NiO + WO_x + $NiWO_4$	4.178 (3)	91
NiW0.45	0.41	38.1	$NiWO_4$ + WO_3	–	nd
NiW0.5	0.47	42.9	$NiWO_4$ + WO_3	–	117
NiW0.7	0.68	29.0	$NiWO_4$ + WO_3	–	110
NiW1	1.0	9.4	WO_3	–	nd

[a] Ni and W contents were determined by atomic absorption spectroscopy.
[b] Determined by XRD and Raman spectroscopy.
[c] Between brackets is the calculated error for the last significant cipher.
[d] Apparent activation energy (in kJ/mol) for the ODH of ethane; nd = not determined.
[e] WO_x could also be nanoparticles of undoped and NiO-doped WO_x.

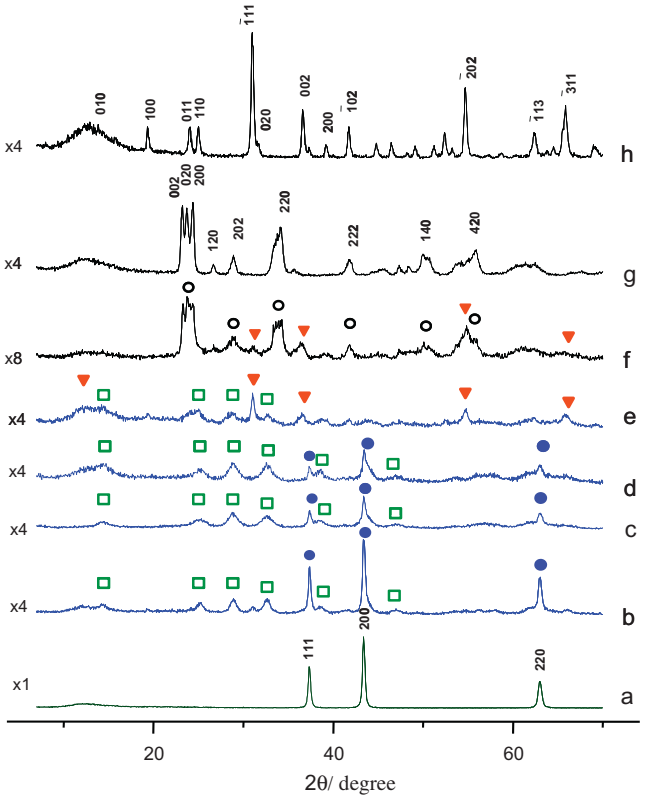

Fig. 1. XRD patterns of Ni–W–O catalysts: (a) NiW0; (b) NiW0.2; (c) NiW0.3; (d) NiW0.36; (e) NiW0.45; (f) NiW0.7; (g) NiW1; (h) $NiWO_4$. Symbols: NiO (●); WO_x (□); $NiWO_4$ (▼); WO_3 monoclinic (○). (For interpretation of the references to colour in this figure legend, the reader is referred to the web version of this article.)

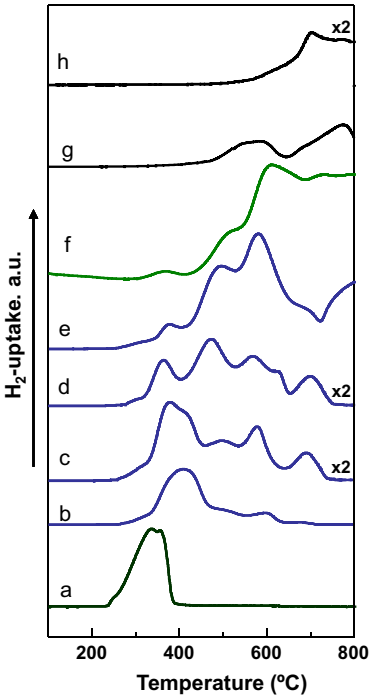

Fig. 2. H_2-TPR curves of Ni–W–O catalysts: (a) NiW0; (b) NiW0.1; (c) NiW0.2; (d) NiW0.3; (e) NiW0.36; (f) NiW0.45; (g) NiW0.7; (h) NiW1.

patterns of W-containing catalysts, which suggests a large decrease in the crystal size of NiO crystals. In the W-rich region (i.e., W/(Ni + W) ratios higher than 0.45), $NiWO_4$ and WO_3 are mainly observed, although the intensity of the corresponding phases depends on the Ni/W ratio.

Fig. 2 shows the TPR patterns of the Ni–W–O catalysts. The W-free sample, NiW0, shows a peak with maximum reduction at ca. 335 °C, attributed to the reduction in bulk NiO according to literature data [23]. A shoulder at 360 °C is also observed, which is probably due to some large particles present in this sample [24].

In W-doped catalyst, i.e., W/(Ni + W) < 0.45, the catalyst reducibility decreases as the maximum NiO reduction peak shifts to higher temperature. The shift of the former peak is likely a consequence of the interaction between NiO particles (with small crystal sizes) and tungsten oxide nanoparticles (surface area significantly increases with W addition) [24]. In addition to this, new bands of less reducible species begin to appear. Thus, the intensity of the band at around 400–460 °C decreases as the tungsten amount is increased, while the intensity of the peaks at higher temperature increases. The reduction peaks appearing at temperatures higher than 460 °C are clearly visible and mainly related to the reduction in tungsten oxide species. However, some contribution of NiO particles with different properties to the reduction bands centered ca. 500 and 600 °C, due to the interaction with surrounding particles of nonstoichiometric tungsten oxide, cannot be rejected (as observed similarity to reported TPR of supported NiO with no reduction event apparently associated with the support) [25,26].

In the case of W-rich samples, i.e., 0.45 < W/(Ni + W) < 0.7, the bands related to the reduction in NiO practically disappear (Fig. 2, patterns f and g). Moreover, the TPR profiles become more complex, since the remaining peaks broaden and strongly overlap, and bands also appear at temperatures higher than 700 °C. In this

way, $NiWO_4$ is clearly observed by XRD, which shows a characteristic reduction peak at ca. 710 °C, as previously described [23]. The Ni-free sample (Fig. 3, pattern h) shows, in agreement with previous work [23,27], a broad band with a shoulder at ca. 600 °C and one peak at ca. 700 °C that spreads beyond 800 °C. These bands are related to the reduction in tungsten oxide forming first W^{5+} species, then W^{4+}, and finally tungsten species with an apparent oxidation number of 2+ (derived from the transformation of the corner-linked WO_6 octahedra along the shear planes into an arrangement of edge-sharing octahedra) [27]. The relative intensities, as well as the temperature of the maxima of these bands, change with the W content, probably due to variations in the WO_x particle size and their interaction with NiO and/or $NiWO_4$ particles.

Accordingly, the incorporation of tungsten favors a partial decrease in the reducibility of Ni sites and the appearance of at least three types of W sites: one is related to WO_x species interacting with NiO and the others to the presence of $NiWO_4$ and monoclinic WO_3, whose intensities depend on the W/(Ni + W) ratio.

The results of XPS analysis of Ni–W–O catalysts are summarized in Table 2. It can be observed that the compositions of bulk and surface are similar for all the catalysts, without a clear outer enrichment of nickel or tungsten.

Fig. 3A shows the Ni2*p*3/2 spectra of the Ni–W–O catalysts. For comparison, the spectra of NiW0 (i.e., W-free NiO) and $NiWO_4$ have also been included (Fig. 3B). In all Ni–W–O samples, the Ni2*p*3/2 XPS main peak shows two additional structures at the high BE side, named satellite peaks: one at −1.5 eV higher BE (Satellite I) and the other at −7 eV higher BE (Satellite II). A similar spectrum is also observed in the NiO sample, as previously reported in the literature [11]. The origin of Satellite I is a matter of controversy. It has been related to the presence of Ni^{3+} ions [28–30], Ni^{2+}–OH species [31], or Ni^{2+} vacancies [32] or to a nonlocal screening mechanism [33–35]. On the other hand, the satellite line at 7 eV higher BE involves

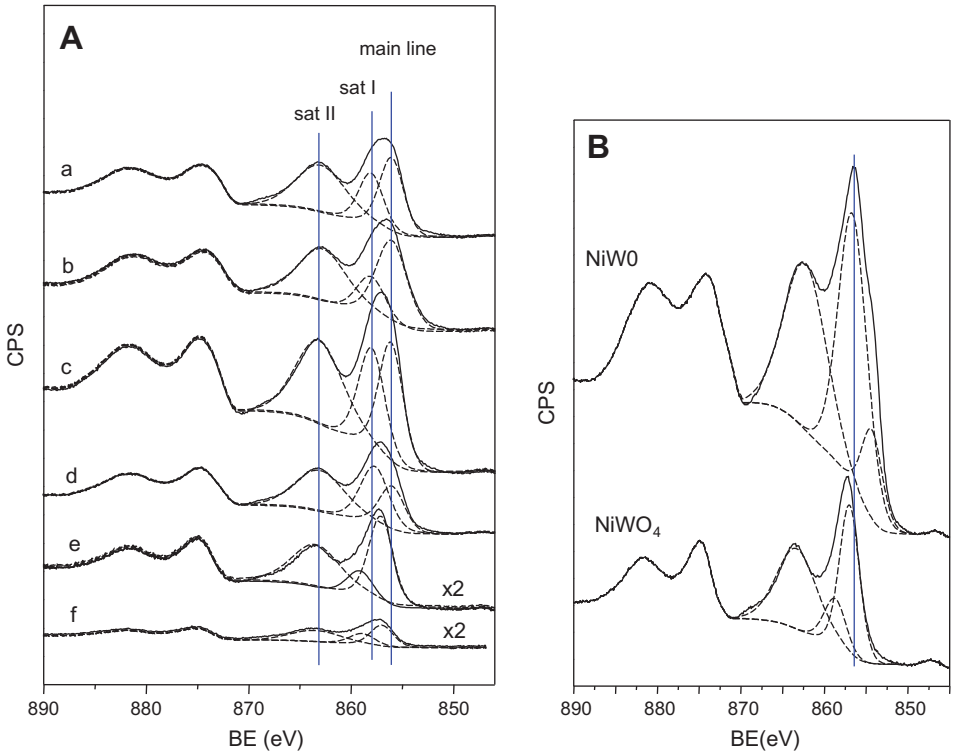

Fig. 3. X-ray photoelectron spectra of Ni2*p*3/2 of Ni–W–O catalysts. (A) (a) NiW0.1; (b) NiW0.2; (c) NW0.3; (d) NiW0.36; (e) NiW0.5; (f) NiW0.7. (B) For comparison, the spectra of NiW0 and $NiWO_4$ are also presented.

Table 2
XPS results for Ni–W–O mixed oxide catalysts.

Sample	W/(Ni + W)	W/(Ni + W)	Ni2*p*3/2					W4*f*7/2	
	Bulk	Surface	Main peak[a] (eV)	Satellite, ΔBE[b] (eV)		Satellite/main-peak intensity ratio		Main peak[a] (eV)	Secondary peak (eV)
				(I)	(II)	(I)	(II)		
NiW0	0	0	854.3	2.3	8.0	4.07	3.9	–	–
NiW0.1	0.09	0.10	856.1	2.0	6.9	0.65	1.28	36.7	37.2
NiW0.2	0.16	0.13	856.0	2.0	6.8	0.41	0.93	36.9	35.7
NiW0.3	0.26	0.20	856.1	1.9	7.0	0.86	1.35	36.5	37.3
NiW0.36	0.33	0.25	856.0	1.7	7.1	1.41	1.83	36.4	–
NiW0.45	0.41	0.51	857.1	2.0	6.4	0.29	0.92	36.4	–
NiW0.5	0.47	0.52	857.1	2.2	6.4	0.24	0.85	36.3	–
NiW0.7	0.68	0.61	857.0	2.0	6.5	0.53	1.21	36.2	37.6
NiW1	1.0	1.0	–	–	–	–	–	36.8	
$NiWO_4$	0.50	0.49	857.0	1.7	6.3	0.32	1.07	36.3	36.6

[a] Estimated experimental error of ±0.1 eV.
[b] BE shift of the satellite peak versus the main peak.

a ligand–metal charge transfer [33–35]. The intensity and position of both satellite lines are very sensitive to the structural arrangement and the nature of the surrounding atoms, giving interesting information about the local environment of the Ni surface atoms.

Table 2 shows the BE of the main line, as well as the separation and intensity ratio of the satellite peaks versus the main peak. A shift to higher BE in the Ni2*p*3/2 XPS main line of Ni–W–O catalysts versus pure NiO is clearly observed, which should be related to the presence of tungsten atoms in the structure of the catalysts. Moreover, in the case of samples with W/(Ni + W) ratios higher than 0.5, the Ni2*p*3/2 BE shifts ca. 1 eV to higher energy (857.0 eV) from the rest of the samples (856.0 eV), which could be related to the presence of $NiWO_4$. Indeed, Raman (not shown here) and XRD results agree with the presence of $NiWO_4$ in Ni–W–O samples with a W/(Ni + W) ratio higher than 0.50. In the case of Ni-rich samples, 0.10 < W/(Ni + W) < 0.36, the BE of the Ni2*p*3/2 XPS main line does not shift significantly, while the intensity and position of both satellite peaks clearly change with increasing tungsten content in the sample. In fact, the satellite (I + II)-main peak intensity ratio follows a Gaussian-type curve vs the tungsten content in the samples, with a maxima at a W/(Ni + W) ratio of 0.30–0.36 (Fig. 4). This could account for a different local environment of the Ni atoms in the bulk structure, influencing the Ni–O interaction.

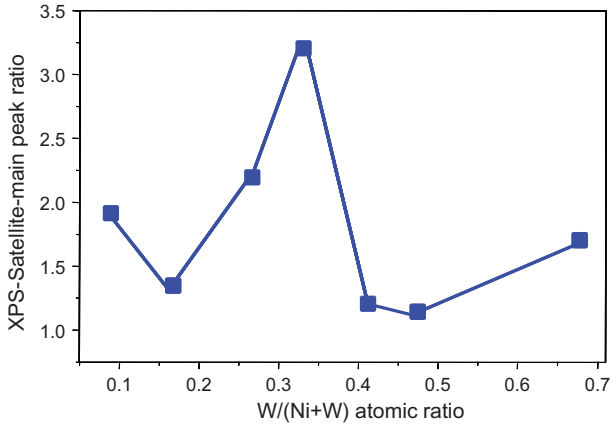

Fig. 4. Variation of the XPS Ni2*p*3/2 satellite (I + II)–main peak intensity ratio with the W/(Ni + W) atomic ratio Ni–W–O mixed oxides.

The W4*f* XPS spectra of the Ni–W–O catalysts, together with those of ***NiW1*** (i.e., NiO-free WO_3) and $NiWO_4$, are shown in Fig. 5. A progressive shift to lower BE in the W4*f*7/2 line, compared with that of bulk WO_3, with increasing tungsten content in the Ni–W–O catalysts is clearly observed (Table 2), which should be related to the presence of Ni atoms in the local environment of W^{6+} species [36,37].

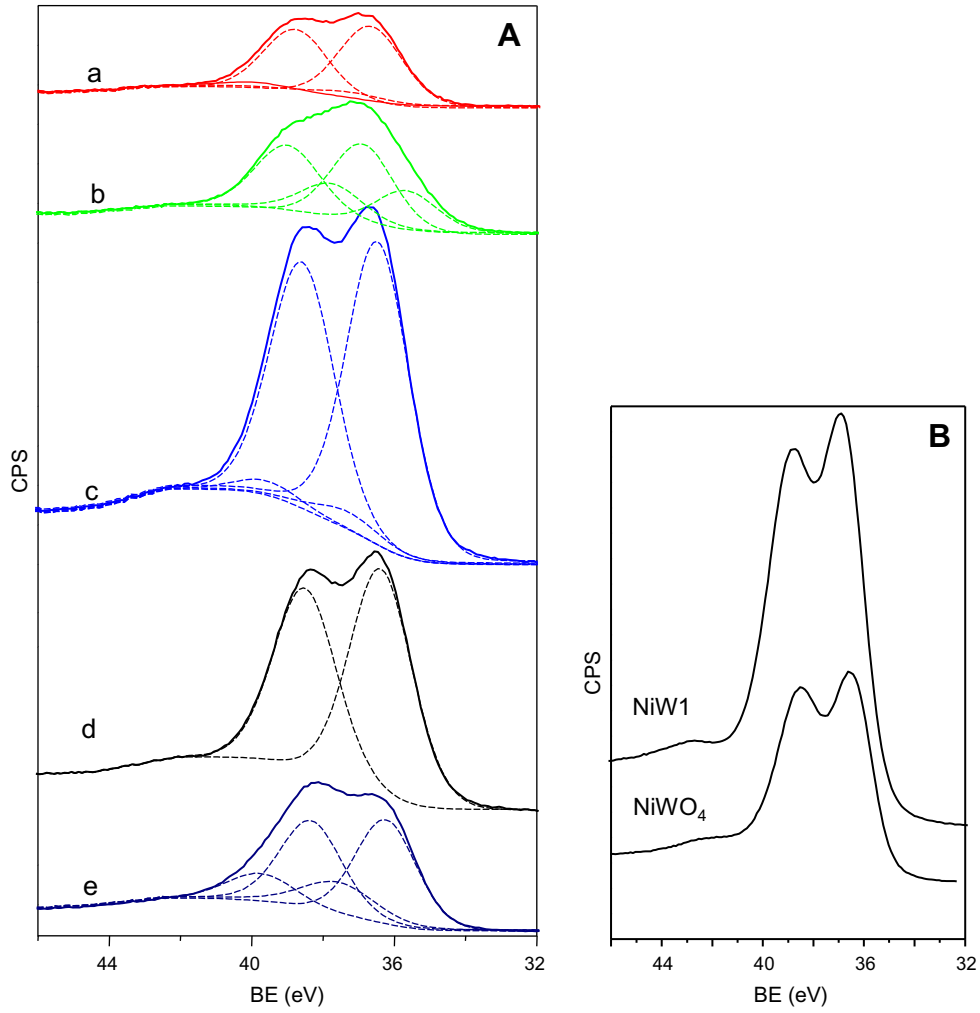

Fig. 5. X-ray photoelectron spectra of W4*f* transition of Ni–W–O catalysts. (A) (a) NiW0.1; (b) NiW0.2; (c) NiW0.3; (d) NiW0.36; (e) NiW0.7. (B) For comparison, the spectra of NiW1 and $NiWO_4$ are also presented.

On the other hand, at a high W/(Ni + W) molar ratio, a W4*f*7/2 BE similar to that observed on $NiWO_4$ is observed. Moreover, a little contribution of W at higher BE (around 37.2 eV) is observed in almost all samples, which could be due to highly dispersed polymeric tungsten species in a different environment, as suggested from the Raman results (not shown).

Since XPS is not a highly surface-sensitive technique, more specific characterization techniques have been chosen to analyze the nature of catalytic surface sites present on the Ni–W–O samples. For this reason, samples with different catalytic behavior have been analyzed by IR spectroscopy of CO adsorption. CO has been widely used for characterization of different types of surface Lewis acid sites, due to the high sensitivity of this molecule. In our study, two samples, named NiW0.36 and NiW0.7, have been selected. For comparison, NiW0, NiW1 and $NiWO_4$ samples have also been analyzed and used as reference compounds.

The IR spectrum in the carbonyl stretching frequency region (2250–2050 cm^{-1}) of the NiW0 sample, i.e., pure NiO, after CO adsorption shows the presence of one intense band at 2153 cm^{-1} (Fig. 6A). The band at 2153 cm^{-1} is associated with CO interacting with OH groups, according to the corresponding shift of the OH groups and the very low stability of the IR band [38]. The absence of Lewis acid sites observed in the NiW0 sample could be related in part to their low surface area. On the other hand, fast hydroxylation of surface sites due to water by cooling of the pellet under the experimental IR procedure has been observed (inset of Fig. 6A), which could also account for the absence of Lewis acid sites detected on this sample.

In the case of pure WO_3, i.e., the NiW1 sample (spectrum not shown), no IR bands associated with carbonyl species are observed after CO adsorption, indicating a small number of Lewis surface sites.

CO adsorption on $NiWO_4$ (Fig. 6B) shows an intense IR band with two components at 2188 and 2176 cm^{-1}, together with another band at 2156 cm^{-1} and a shoulder at 2140 cm^{-1}. The IR band at 2188 cm^{-1} is related to CO interacting with Lewis acid sites, the 2176 and 2156 cm^{-1} IR bands are associated with CO interacting with OH groups, according to the respective shift in the OH groups, and the 2140 cm^{-1} IR band is due to physisorbed CO. The greater shift of the CO frequency in the 2176 cm^{-1} IR band compared with the 2156 cm^{-1} band points to higher acidity of the OH group in the former. Indeed, two hydroxyl groups at 3666 and 3631 cm^{-1} are observed in the OH region, which are shifted due to CO adsorption, giving rise to the corresponding 2176 and 2156 cm^{-1} IR bands.

On the NiW0.36 sample, two intense IR bands at 2189 and 2156 cm^{-1} together with a shoulder at 2143 cm^{-1} are observed (Fig. 6C). The shoulder at 2143 cm^{-1} is ascribed to physisorbed CO. The IR band at 2156 cm^{-1} can be assigned to CO interacting with OH groups [38], while the higher frequency band at 2189 cm^{-1} is associated with CO interacting with Lewis acid sites on the catalysts' surface [39,40].

On the NiW0.7 sample, three IR bands are observed at 2200 cm^{-1}, associated with Ni^{2+} Lewis acid sites, 2164 cm^{-1}, associated with OH groups according to the corresponding shift in the hydroxyl region, and 2143 cm^{-1}, due to physisorbed CO (Fig. 6D).

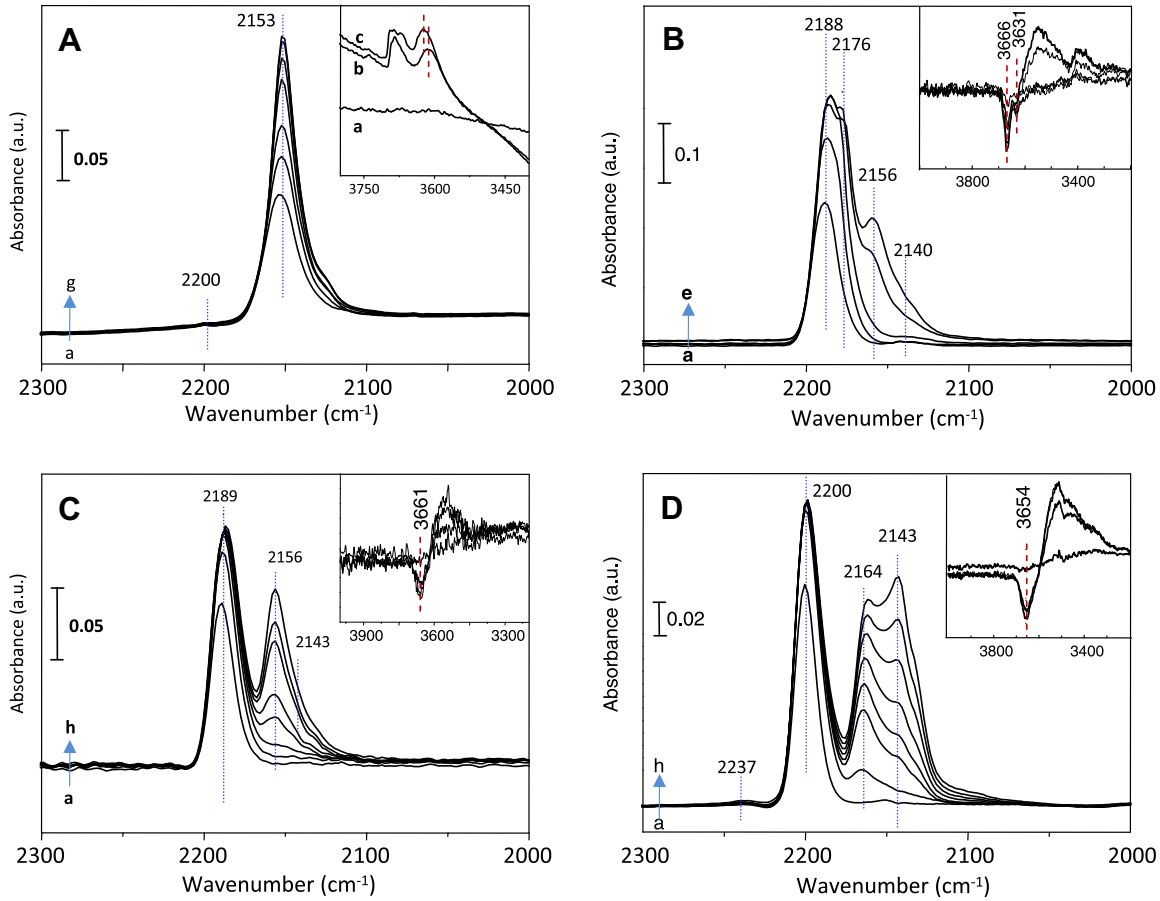

Fig. 6. FTIR spectra at −176 °C of NiW0 (A), $NiWO_4$ (B), NiW0.36 (C), and NiW0.7 catalysts (D) after CO adsorption at increasing coverage (a–g or a–h, 0.4–8.5 mbar). Inset in (A): IR spectra in the hydroxyl region of (a) NiO sample after activation at 250 °C, (b) after cooling down to 25 °C, (c) after 8.5 mbar CO adsorption. Inset in (B–D): changes in the IR spectra in the hydroxyl region after 8.5 mbar CO adsorption.

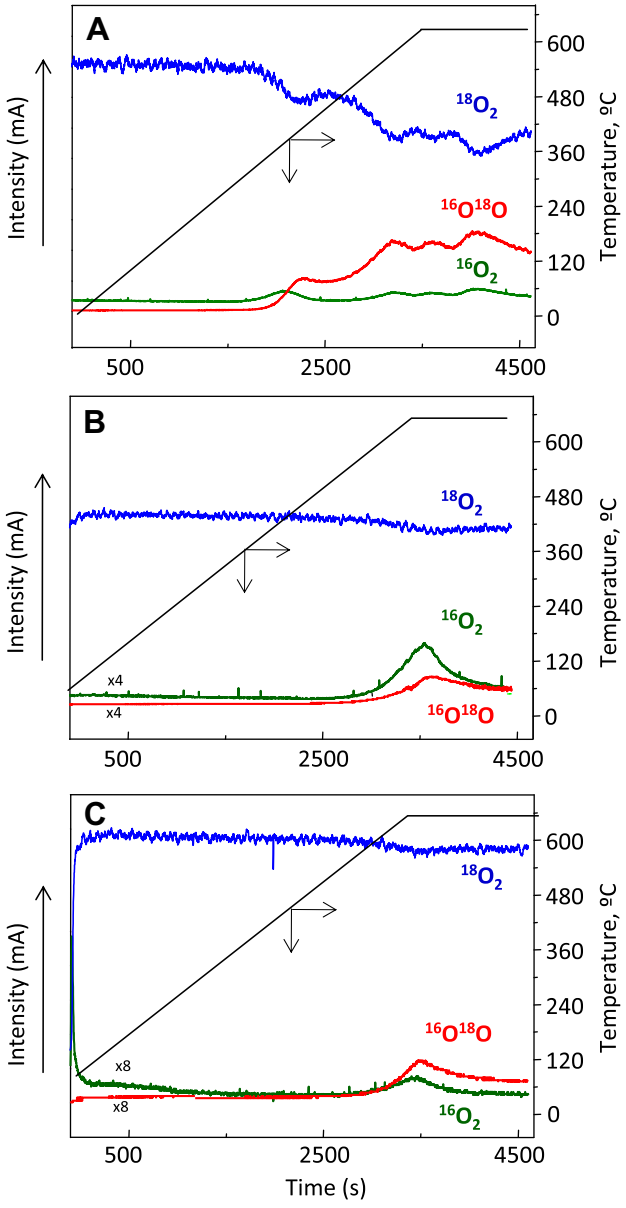

Fig. 7. Temperature-programmed $^{18}O_2$ isotopic oxygen exchange profiles of NiW0 (A), NiW0.36 (B), and NiW0.7 (C).

According to the IR spectra, the presence of tungsten in the Ni–W–O samples leads to the formation of Lewis and Brønsted acid sites. The Lewis acidity of the samples increases in the order Ni-WO_4 = NiW0.36 (2186 cm^{-1}) < NiW0.7 (2200 cm^{-1}), while the Brønsted acidity increases as follows: NiO (2153 cm^{-1}) < NiW0.36 (2156 cm^{-1}) < NiW0.7 (2164 cm^{-1}) < $NiWO_4$ (2156 and 2176 cm^{-1}). The higher acidity of surface sites could explain the appearance of consecutive reactions during the oxidation of ethane over W-containing samples, as will be shown later.

On the other hand, temperature-programmed $^{18}O_2$ isotope-exchange measurements (TPIE) make it possible to investigate the nature of oxygen species participating in the reaction mechanism and the type and density of surface sites available for oxygen activation. Indeed, the distribution of isotopic-exchange products ($^{16}O_2$ and $^{16}O^{18}O$) depends on the relative rates of oxygen dissociation, surface exchange, lattice incorporation, and diffusion into the bulk [14]. Thus, fast oxygen dissociation followed by rapid surface oxygen exchange compared with the oxygen diffusion rate into the bulk leads to the formation of $^{16}O^{18}O$, while a faster incorporation reaction and subsequent diffusion step into the bulk result in $^{16}O_2$ as the dominant product [41]. The TPIE profiles in the temperature range 25–650 °C for NiW0, NiW0.36, and NiW0.7 samples are shown in Fig. 7. The oxygen isotopic-exchange process starts at a lower temperature (320 °C) on the NiW0 sample than on the Ni–W–O mixed oxides (500 °C), indicating that the reactivity of exchangeable oxygen species is higher on the W-free sample (NiW0) than those achieved for W-containing samples. This agrees with a greater ability of the NiW0 sample for oxygen activation (i.e., dissociation) and a higher activity of these oxygen species.

The amount of exchangeable oxygen species ($^{16}O_2$ and $^{16}O^{18}O$) normalized to Ni atoms is shown in Fig. 8. On the NiW0 sample, rapid surface oxygen exchange is observed, which can be attributed to fast oxygen dissociation on surface defects, leading to the formation of highly active surface oxygen species. In agreement with the TPIE results, the dissociation of oxygen on surface defects is eliminated by the incorporation of tungsten into the catalyst. In addition, the reactivity of surface oxygen species is decreased, according to the higher T_{onset} for oxygen exchange. This agrees with TPR results in which the addition of W species decreases the reducibility of Ni surface sites. On the other hand, different distributions of isotopic oxygen species are observed on both NiW0.36 and NiW0.7 samples. Larger amounts of doubly exchanged oxygen species ($^{16}O_2$) compared with cross-labeled oxygen species ($^{16}O^{18}O$) are observed on the NiW0.36 sample,

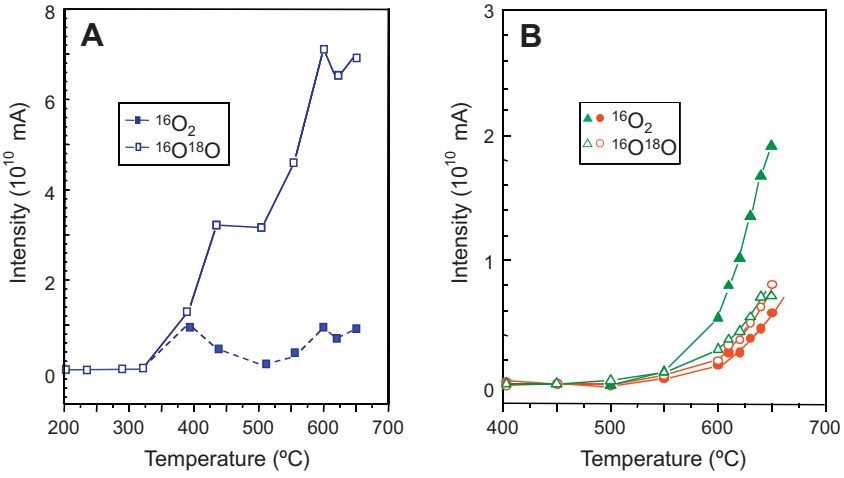

Fig. 8. Evolution of the oxygen exchange species per Ni atom during TPIE experiments on NiW0 (■, □), NiW0.36 (▲, △), and NiW0.7 (●, ○) catalysts. Symbols: $^{16}O_2$ (■, ▲, ●); $^{16}O^{18}O$ (□, △, ○). (For interpretation of the references to colour in this figure legend, the reader is referred to the web version of this article.)

indicating faster diffusion of oxygen into the bulk and a smaller amount of oxidizing surface oxygen species. However, the prevalent formation of cross-labeled oxygen species for NiW0.7 indicates the presence of a larger amount of surface oxidizing species than of doubly exchanged oxygen species in the same catalyst. This type of surface oxygen species has been referred to in the literature as electrophilic oxygen species and as responsible for CO_2 formation [14].

3.2. Catalytic performance in ethane oxidation

Fig. 9 shows the variation of ethane conversion with the reaction temperature achieved over Ni–W–O mixed oxide catalysts. It can be seen that the temperature necessary to achieve 10% ethane conversion increases from the NiW0 sample at ca. 310 °C to more than 450 °C for samples with W/(Ni + W) atomic ratios of 0.36 and higher.

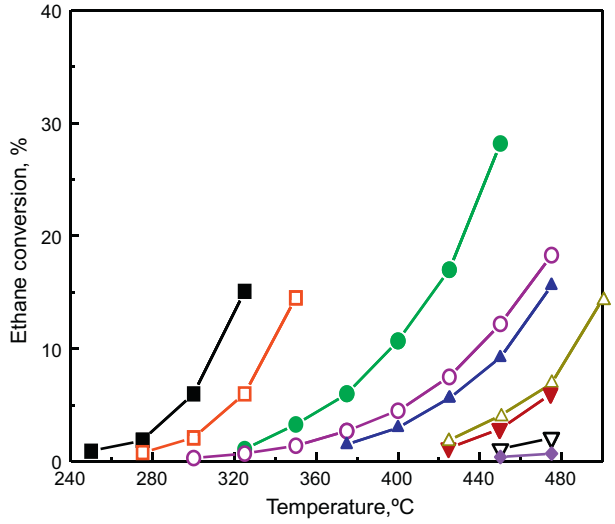

Fig. 9. Variation of ethane conversion with the reaction temperature during the oxidation of ethane over Ni–W–O mixed oxides. Symbols: NiW0 (■); NiW0.1 (□); NiW0.2 (●); NiW0.3 (○); NiW0.36 (▲); NiW0.45 (△); NiW0.5 (▼); NiW0.7 (▽); NiW1 (♦). (For interpretation of the references to colour in this figure legend, the reader is referred to the web version of this article.)

Fig. 10 shows the variation of the rate of formation of ethylene per unit mass of catalyst (STY_{C2H4}, in $g_{C2H4}\ h^{-1}\ g_{cat}^{-1}$), the activity per gram of nickel (in $g_{C2H6}\ s^{-1}\ g_{Ni}^{-1}$), and the catalytic activity per Ni atom normalized per surface area of catalyst (in $g_{C2H6}\ Ni^{-1}\ m^{-2}\ h^{-1}$) with the W content in Ni–W–O catalysts. It can be observed that in all three cases, the activity (per mass of catalyst, per surface area, or per both mass and surface area) decreases when the tungsten loading of the catalyst increases. Therefore, the catalytic activity of these catalysts depends on something apart from the surface area and the amount of nickel.

Fig. 11 shows the variation of the selectivity to ethylene with the ethane conversion achieved on Ni-rich (Fig. 11a) and W-rich (Fig. 11b) catalysts. A completely different pattern is observed for the two types of catalysts. In the case of Ni-rich catalysts, i.e., $0 < W/(Ni + W) < 0.36$ (Fig. 11a), the initial selectivity to ethylene (selectivity at very low ethane conversion) increases with increasing W content. Furthermore, in the range of ethane conversion studied, these catalysts do not show appreciable variation of the selectivity to ethylene with the ethane conversion, except in the case of samples NiW0.3 and NiW0.36 (the most selective catalysts), in which a very small decrease in selectivity to ethylene takes place with ethane conversion (the selectivity to ethylene drops from ca. 60% to ca. 50% when the ethane conversion is increased from 5% to 35%). It is clear that in this case, the reaction network can be explained by parallel and consecutive reactions (Scheme 1a), in which the incorporation of small amount of W atoms favors a decrease in k_2 and an increase in the k_1/k_2 ratio.

In the case of W-rich catalysts, i.e., samples with $0.45 < W/(Ni + W) < 1$ (Fig. 11b), the initial selectivity to ethylene (at very low ethane conversion) is very high in all cases. In addition, the selectivity to ethylene decreases with the ethane conversion (this loss of selectivity is also greater when the amount of W in the catalyst is increased). On the other hand, in this type of catalyst, a reaction network based on both parallel and consecutive reactions can be proposed (Scheme 1b), in which k_2 is very low and the k_3/k_1 ratio increases with increasing W loading. The initial selectivity reaches a maximum for a W/(Ni + W) atomic ratio of about 0.5, although for this catalyst an important selectivity loss with ethane conversion is observed. In any case, the best behavior at high

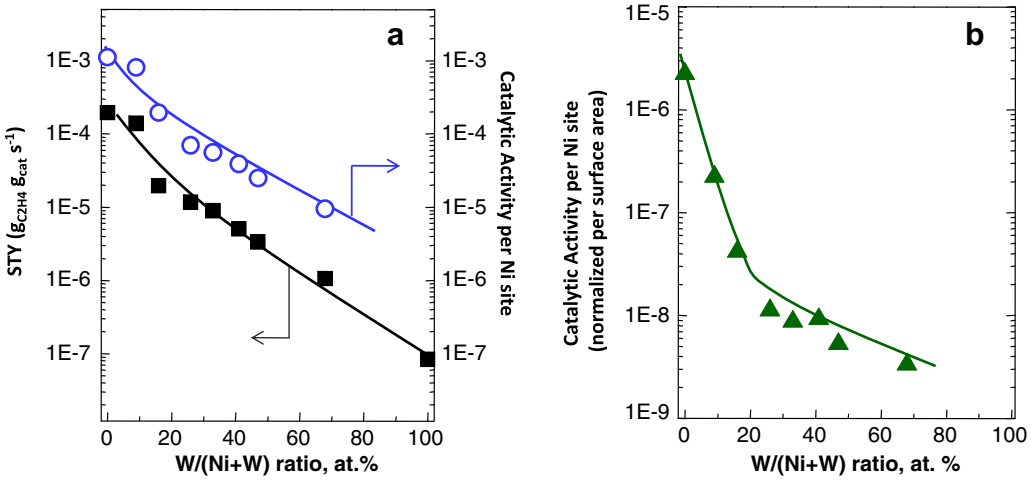

Fig. 10. Variation of the formation rate of ethylene, STY (in $g_{C2H4}/g_{cat}/h$) (■), catalytic activity for ethane conversion normalized gram of nickel (in $g_{C2H6}\ g_{Ni}^{-1}\ h^{-1}$) (○), and catalytic activity for ethane conversion per Ni atom normalized per surface area of catalyst (in $g_{C2H6}\ Ni^{-1}\ m^{-2}\ h^{-1}$) (▲) with the W content of catalysts achieved during the ODHE over Ni–W–O catalysts at 425 °C. (For interpretation of the references to colour in this figure legend, the reader is referred to the web version of this article.)

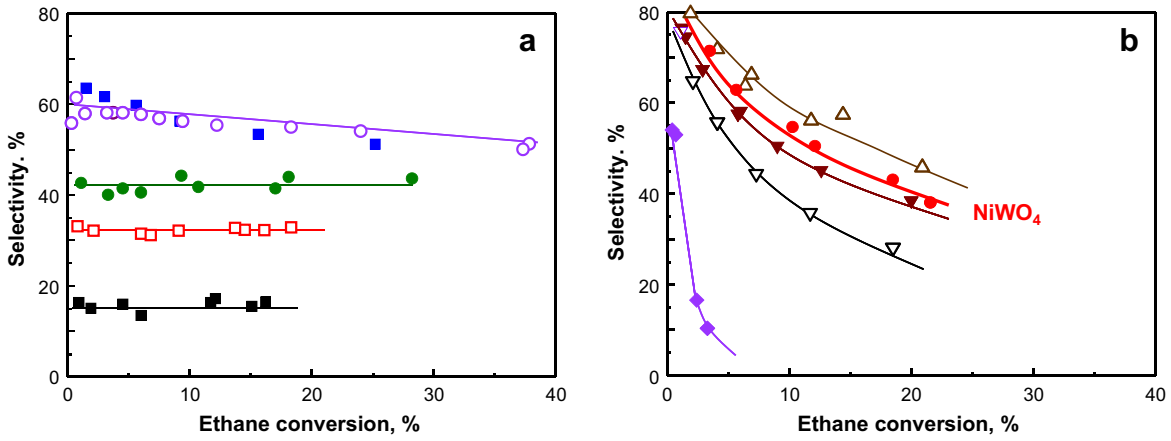

Fig. 11. Variation of selectivity to ethylene with the ethane conversion achieved at 400 °C over Ni-rich (a) and W-rich (b) catalysts. Symbols: NiW0 (■); NiW0.1 (□); NiW0.2 (●); NiW0.3 (○); NiW0.36 (■); NiW0.45 (△); NiW0.5 (▼); NiW0.7 (▽); NiW1 (♦). For comparison, the results achieved over pure NiWO4 (●) have also been included. (For interpretation of the references to colour in this figure legend, the reader is referred to the web version of this article.)

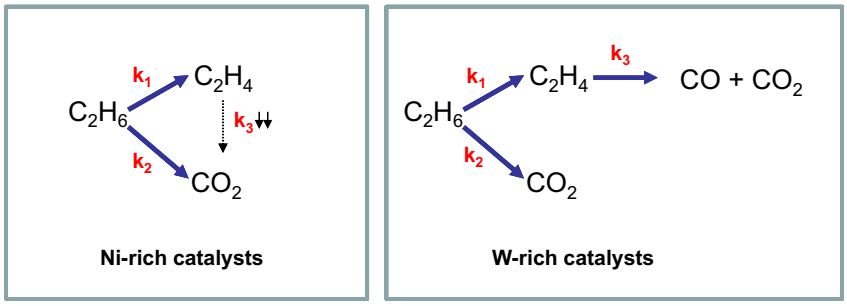

Scheme 1. Reaction networks for the oxidative dehydrogenation of ethane over Ni-rich and W-rich Ni–W–O catalysts.

ethane conversion is obtained for catalysts with lower tungsten content, in which the W/(Ni + W) ratio is between 0.30 and 0.36.

Fig. 12 shows the variation of the selectivity to ethylene, CO, and CO_2 on four characteristic catalysts. The sample with low W loading, NiW0.2, shows no influence of the ethane conversion on the selectivity to ethylene and CO_2, and the formation of CO is not observed. However, over NiW0.36, a small decrease in the selectivity to ethylene with ethane conversion can be seen, while the formation of CO is clearly observed (especially at high ethane conversion).

Finally, for samples with higher W loading, i.e., NiW0.5 and NiW0.7, the formation of CO clearly increases with ethane conversion and the W loading of the catalyst, while the selectivity to ethylene presents an opposite trend (Fig. 12). According to these results, it can be said that CO is mainly formed from ethylene, by consecutive oxidation, ethylene is formed directly from ethane and CO_2 can be formed either from ethane (main) or from ethylene decomposition. However, the extension of parallel and consecutive reactions strongly depends on the W/(Ni + W) ratio in the catalyst.

The apparent activation energy for the direct transformation of ethane to ethylene over Ni–W–O catalysts is shown in Table 1. The apparent energy for ethylene formation varies depending on the catalyst (from 91 to 117 kJ mol^{-1} for catalysts with a W/(Ni + W) ratio between 0.20 and 0.36, those that present the lowest energies, similar to that observed for NiO).

Similar apparent activation energy for ethane oxidation to ethylene has also been reported for Ni–Nb–O catalyst (96.2 kJ mol^{-1}) [14], although the apparent activation energy for ethane oxidation to CO_2 was lower than that observed in our catalysts. This could explain the different behavior with reaction temperature.

3.3. Catalytic performance in ethylene oxidation

Ethylene oxidation experiments have been conducted on some representative Ni-rich (NiW0.2 and NiW0.3) and W-rich (NiW0.5 and NiW0.7) catalysts (Table 3). CO and CO_2 were only detected as reaction products, although the relative amount of each carbon oxide was demonstrated to depend on the catalyst composition. Thus, the Ni-rich catalyst (NiW0.2) showed mainly CO_2 with selectivity 98–100%. The selectivity to CO_2 achieved by the NiW0.3 sample was ca. 75%; for samples NiW0.5 and NiW0.7, it was ca. 45% and ca. 30%, respectively. Thus, it can be observed that the higher the W content of the catalyst the lower was the selectivity to CO_2 obtained. It must be mentioned that the selectivity to the different carbon oxides obtained remained almost constant regardless of the ethylene conversion, suggesting that (i) CO and CO_2 are primary products and (ii) CO_2 is not formed by the further oxidation of CO.

Table 3 compares the catalytic activity for ethane and ethylene oxidation. It can be seen that in Ni-rich samples, the relative activity between ethane and ethylene oxidation is much higher than that achieved over W-rich catalysts. While the ethylene conversion is similar on NiW0.2, NiW0.3, and NiW0.5 (and only twice more reactive than on NiW0.7), the ethane conversion greatly decreases in all cases when the tungsten loading increases (the reactivity of NiW0.2 is more than 20 times higher than that of NiW0.7). Therefore, the different selectivity to ethylene observed over these catalysts in the ODHE can be explained by the large differences in the catalytic activation of ethane over Ni-rich samples with respect to those achieved over W-rich samples.

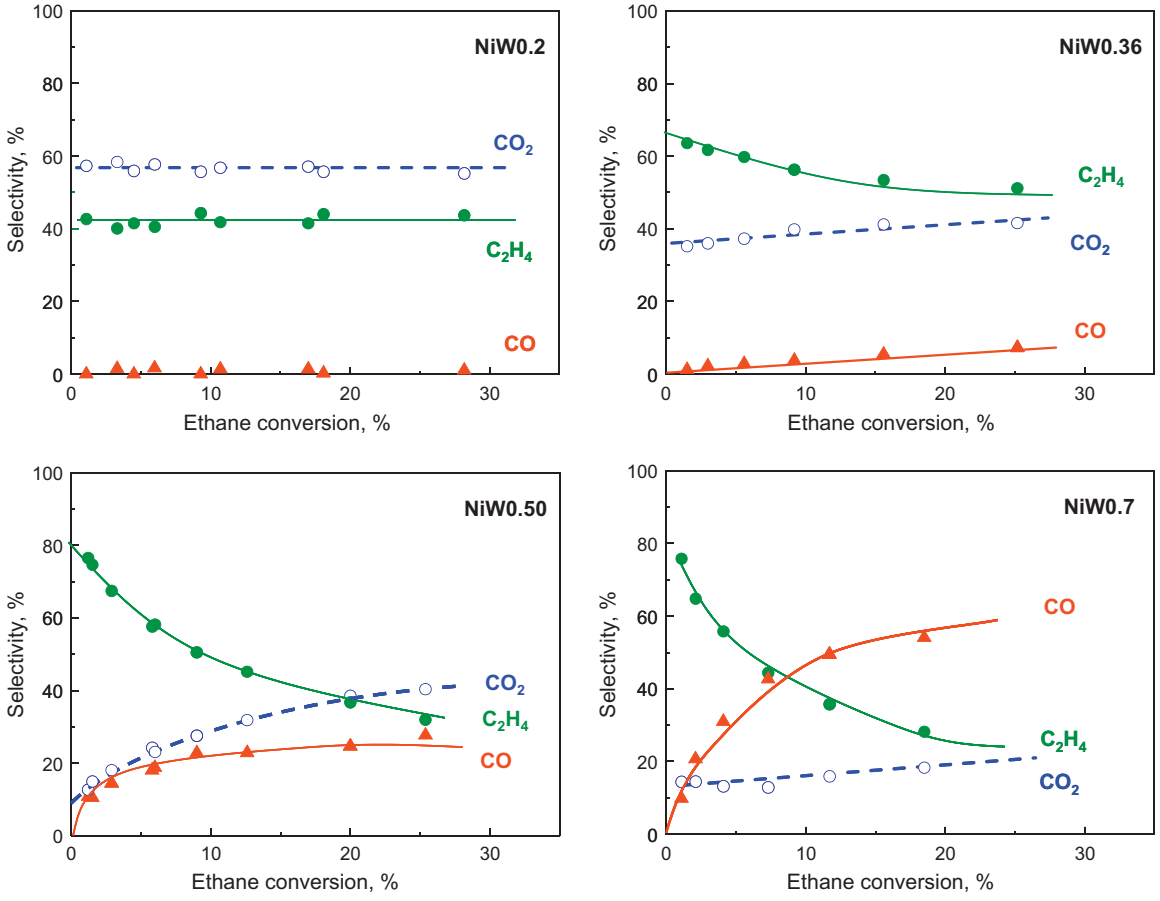

Fig. 12. Variation of selectivity to ethane (●), CO (▲), and CO_2 (○) with the ethane conversion achieved at 400 °C over Ni–W–O catalysts: NiW0.2, NiW0.36, NiW0.5, and NiW0.7. Experimental conditions in text. (For interpretation of the references to colour in this figure legend, the reader is referred to the web version of this article.)

Table 3
Catalytic activity for ethane and ethylene oxidation over Ni–W–O mixed oxide catalysts.

Catalyst	Ethylene oxidation [a]		Catalytic activity [b]		Relative activity (ethane/ethylene)
	Selectivity[c] (%)		Ethylene (10^3 mol_{C2H4} g_{cat}^{-1} h^{-1})	Ethane (10^3 mol_{C2H6} g_{cat}^{-1} h^{-1})	
	CO_2	CO			
NiW0.2	99	1	1.54	7.4	4.8
NiW0.3	75	25	1.10	3.7	3.7
NiW0.5	48	52	1.45	0.87	0.60
NiW0.7	29	71	0.60	0.32	0.53

[a] Reaction conditions in text, reaction temperature = 425 °C.
[b] Catalytic activity for ethylene or ethane oxidation at 425 °C.
[c] The selectivity to carbon oxides is almost constant in the conversion range studied (until 15%).

3.4. General remarks

The interaction of NiO with other metal oxides can improve the catalytic properties of NiO during the oxidative dehydrogenation of ethane. This is the case for NiO supported on Al_2O_3 [10,11,21] and MgO [17], in which it is possible to achieve selectivity to ethylene higher than that observed over pure NiO. However, as a consequence of the interaction between the support and NiO particles, lower catalytic activity for ODHE is observed over supported catalysts, especially in NiO/MgO, for which reaction temperatures higher than 500 °C are required. The higher selectivity achieved over alumina-supported NiO catalysts, with high ethane reactivity at reaction temperatures lower than 450 °C, has been related to the low affinity of this catalyst for ethylene oxidation [11] or to a selective partial elimination of one of the two types of active oxygen species present in NiO [10,42]. In this way, TPD-O_2 experiments on NiO/Al_2O_3 catalysts suggested the partial elimination of the more reactive (and unselective) oxygen species without modification of the less active but more selective ones [11].

A similar mechanism has been proposed for Nb-promoted NiO catalysts [13,14,19,20], although it leads to higher production of ethylene. The incorporation of Nb into the NiO lattice (by substitution of nickel atoms and/or filling of the cationic vacancies in the defective nonstoichiometric NiO surface) favors a partial reduction in the nonstoichiometric NiO crystals abundant on pure nickel oxide and responsible for the total oxidation of ethane to carbon dioxide [13]. This has been confirmed by SSITKA (steady state isotopic transient kinetic analysis) experiments with isotopic $^{18}O_2$ [14], suggesting that the dissociation of oxygen, leading to a high concentration of intermediate electrophilic oxygen species on the

surface, is the fast step of the exchange process in pure NiO. These electrophilic oxygen species are active for the total oxidation of ethane. However, doubly exchanged species were mainly observed on the Ni–Nb–O catalyst, which suggest that Nb cations in NiO favor the diffusion of oxygen species in the bulk of the catalyst and increase the presence of nucleophilic oxygen species (also decreasing the presence/formation of the most oxidizing species). The importance of nucleophilic oxygen species for oxidative dehydrogenation of lower alkanes has been proposed in recent years [3–5,14–16].

The catalytic results over Ni–W–O mixed oxides show different catalytic performance depending on the W/(Ni + W) ratio of the catalysts, which is related to the different characteristics of the active sites in these materials. In fact, the presence of tungsten in Ni–W–O catalysts strongly modifies the nature of active phases and the characteristics of active and selective sites on the surfaces of the catalysts compared with pure NiO. Fig. 10 shows the evolution of the formation rate of ethylene per unit mass of catalyst (STY_{C2H4}) and the activity per gram of nickel with the W content of catalysts, achieved during the ethane oxidation. As can be observed, both the formation of the olefin and the catalytic activity for ethane oxidation normalized per nickel content decrease when the W loading increases. Since WO_3 has been shown to present extremely low activity, Ni–O sites can be considered as the active centers for the selective activation of ethane over Ni–W–O catalysts, although the intrinsic catalytic activity of Ni sites decreases in W-containing samples.

XP spectra have demonstrated that the concentration of Ni near the surfaces of the catalysts is quite similar to that of the bulk, and therefore, the number of available sites on the surface will depend, apart from the surface area, on the amount of nickel in the catalyst. However, the different characteristics of the Ni species must be an important factor in the catalytic behavior of these catalysts. Also, a modification of the Ni species (variations in the oxidation state and/or coordination) was observed by the XPS technique when the W content in the catalyst increased (Fig. 5).

Taking into account that redox is the most likely mechanism for the ODHE reaction on these catalysts, lower catalyst reducibility would account for the decrease in the activity per nickel site. TPR profiles show a modification of the catalyst reducibility that explains the low catalytic activity of the W-rich catalysts (a decrease in both catalytic activity and catalyst reducibility was observed when the W content increased). This is also confirmed by the oxygen isotope-exchange experiments, in which the number and activity of exchangeable oxygen species decrease considerably upon the addition of tungsten oxide to NiO.

On the other hand, IR spectra of CO adsorption show a different nature of Lewis acid sites in the Ni–W–O catalysts depending on the W content. Indeed, higher acidity of both surface Lewis acid sites and OH groups is observed in samples with high W content (sample NiW0.7), although it is not observed for pure WO_3 sample. Accordingly, the addition of tungsten to the catalysts changes the nature of the Ni species, increases both the number of Lewis acid sites and the diffusion rate of oxygen species into the bulk of the catalyst, and decreases the presence of highly active (i.e., electrophilic) surface oxygen species. All these changes can favor a higher selectivity to ethylene, decreasing the number of deep oxidation sites in catalysts.

In the Ni-rich Ni–W–O catalysts, the selectivity to ethylene increases while that to CO_2 decreases as the tungsten loading increases. In this case, the formation of CO is negligible and the selectivity to ethylene remains almost constant with the ethane conversion. This suggests that deep oxidation of the ethylene formed does not occur or takes place to a low extent (see Scheme 1, left). In agreement with the characterization results, NiO crystals are mainly observed in Ni-rich catalysts (although the XRD patterns show lower intensity of the corresponding reflections), while polymeric WO_x species can also be deduced from the XRD and Raman spectra (not shown here). High surface areas have also been observed in catalysts with W/(Ni + W) ratios of 0.30 and 0.36. Accordingly, these catalysts can be described as NiO in which part of the unselective sites is eliminated by the deposition of polymeric tungsten species and/or WO_x crystals. Indeed, oxygen isotope experiments have shown a strong decrease in the number of surface exchange oxygen species. On the other hand, XPS results show differences in the coordination environment of Ni atoms according to their satellite structure. Maximum selectivity has been observed in samples with maximal satellite-main peak intensity ratio. Finally, the number of acids sites increases with the W content (Fig. 6).

In the case of W-rich catalysts, WO_3 and $NiWO_4$ are mainly observed, the first increasing at higher W/(Ni + W) ratios and the second presenting an opposite trend. It is clear that Ni^{2+} species in $NiWO_4$ are active and relatively selective, while WO_3 shows low activity and low selectivity. However, as a consequence of the presence of different active phases, these catalysts are active in both ethane and ethylene oxidation, and deep oxidation of ethylene to CO is also observed. Accordingly, a reaction pathway as that shown in Scheme 1 (right), with both parallel and consecutive reactions, can be proposed. The presence of polytungstate species on the surface of the catalysts can also contribute to improve the selectivity to ethylene in catalysts with W/(Ni + W) ratios between 0.5 and 0.7. However, the presence of WO_3 in catalysts with higher W loadings should have a little influence on catalytic behavior, as suggested by the extremely low activity achieved over pure WO_3, while $NiWO_4$ is relatively active in both ethane ODH and ethylene deep oxidation (Fig. 9b). We must note that the ratio between ethane oxidation and ethylene oxidation for the NiW0.7 sample (ca. 0.5) is much lower than those observed for catalysts with low W loading (ca. 4.8).

On the other hand, it has been proposed for Ni–Nb–O catalysts that, apart from improving the dispersion of the nickel phase, niobium facilitates C–H bond activation by acting as an electron transfer promoter [13]. This behavior could also be proposed in our case.

In a recent article, the Me-valence in Ni–Me–O mixed oxides has been demonstrated to be of paramount importance for the characteristics of the catalysts and consequently for catalytic performance during ethane oxidative dehydrogenation [15]. Without going into detail, it can be said that high Me valences favor the formation of ethylene. In our case, tungsten is mainly present as W^{6+}: (i) as WO_x in Ni-rich catalysts or (ii) as $NiWO_4$ and WO_3 in W-rich catalysts. Thus, W^{6+} is assumed to be an interesting promoter of NiO at W/(Ni + W) atomic ratios in the range 0.3–0.4.

Finally, it has been proposed that an efficient catalyst for the ODH reaction should achieve a compromise between the ability to activate the C–H bond and the ability to release olefin [43]. Accordingly, one selective catalyst could be prepared by optimizing the ethane activation and facilitating the ethylene desorption, although other possibilities must be considered. Thus, one strategy could be the selective elimination of deep oxidation of ethane without the formation of new actives sites which could favor the deep oxidation of ethylene and try to optimize the acidity of Lewis surface sites, in order to favor activation of the alkane but avoid readsorption of the olefin. This is the case of Ni–W–O mixed oxide and maybe in part in Ni–Nb–O, in the Ni-rich region, with Ni^{2+} sites in W-doped NiO. However, this is not observed in Ni–W–O mixed oxide in the W-rich region, with Ni^{2+} sites in a less active phase (i.e., $NiWO_4$), which is also active in ethylene oxidation.

4. Conclusions

The results of this study show that Ni–W–O mixed oxides are active and relatively selective in the oxidative dehydrogenation of ethane. Ni–O sites seem to be the active species in these catalysts, although the nature of crystalline phases, the environment of Ni sites (as well as their physicochemical characteristics), and the catalytic behavior strongly depend on the catalyst composition.

Pure NiO shows a low selectivity to ethylene but remains almost constant when the ethane conversion is increased. This is consistent with the fact that it shows a higher reducibility and a greater amount of exchangeable oxygen species than observed for Ni–W–O samples. On the other hand, pure $NiWO_4$ and especially WO_3 present high initial selectivity to ethylene, which rapidly drops when the ethane conversion increases.

For W-rich N–W–O catalysts, the presence of $NiWO_4$ and WO_3 in different proportions, depending on the W content of the catalyst, determines their catalytic behavior. Moreover, the presence of Lewis acid sites, with relatively high acid strength, facilitates the consecutive decomposition of the ethylene formed during the ethane oxidation. Thus, the decrease in the selectivity to ethylene with ethane conversion is greater at high W content.

For Ni-rich catalysts, i.e., with $0.1 < W/(Ni + W) < 0.4$, intermediate catalytic behavior is observed. The catalytic activity for ethane oxidation decreases (and the selectivity to ethylene increases) with the tungsten loading as a consequence of the lower reducibility and smaller amount of the Ni–O sites on the catalyst surface. However, no influence of ethane conversion on the selectivity to ethylene is clearly observed (and a very low selectivity to CO is observed in the ethane conversion range studied). The characterization results presented here suggest that small NiO particles and WO_x nanoparticles are mainly present, although polymeric tungstate species could also be present in samples with higher W content. The interaction of NiO particles with WO_x nanoparticles seems to be an important factor in the improvement of the selectivity to ethylene, probably blocking the active and nonselective sites of pure nickel oxide, similarly to Ni–Nb–O catalysts.

According to these results, it has been concluded that both parallel and consecutive reactions (including selective and nonselective steps) in this reaction can be tuned by changing the Ni/W ratio in the catalysts.

Acknowledgments

Financial support from DGICYT in Spain (Project CTQ-2009-14495) and Generalitat Valenciana (ACOMP/2010/091) is gratefully acknowledged.

References

[1] D.N. Nakamura, Oil Gas J. 107 (28) (2009) 43.
[2] T. Ren, M.K. Patel, K. Blok, Energy 33 (2008) 817.
[3] F. Cavani, N. Ballarini, A. Cericola, Catal. Today 127 (2007) 113.
[4] J.M. López Nieto, Top. Catal. 41 (2006) 3.
[5] H.X. Dai, C.T. Au, Curr. Top. Catal. 3 (2002) 33.
[6] G. Grubert, E. Kondratenko, S. Kolf, M. Baerns, P. Van Greem, R. Parton, Catal. Today 81 (2003) 337.
[7] M.D. Argyle, K. Chen, A.T. Bell, E. Iglesia, J. Phys. Chem. B 106 (2002) 5421.
[8] J.M. López Nieto, P. Botella, M.I. Vázquez, A. Dejoz, Chem. Commun. (2002) 1906.
[9] P. Botella, E. García-González, A. Dejoz, J.M. López Nieto, M.I. Vázquez, J. González-Garcia, J. Catal. 225 (2004) 428.
[10] X. Zang, J. Liu, J. Xie, Appl. Catal. A 240 (2003) 143.
[11] E. Heracleous, A.F. Lee, K. Wilson, A.A. Lemonidou, J. Catal. 231 (2005) 159.
[12] (a) Liu, US Patent 6891,075, 2005;
(b) Y. Liu, US Patent 7227,049 A2, 2007.
[13] E. Heracleous, A.A. Lemonidou, J. Catal. 237 (2006) 162.
[14] E. Heracleous, A.A. Lemonidou, J. Catal. 237 (2006) 175.
[15] E. Heracleous, A.A. Lemonidou, J. Catal. 270 (2010) 67.
[16] B. Savonova, S. Loridant, D. Filkova, J.M.M. Millet, Appl. Catal. A 390 (2010) 148.
[17] K.-I. Nakamura, T. Miyake, T. Konishi, T. Suzuki, J. Mol. Catal. A 260 (2006) 144.
[18] M.L. Rodriguez, D.E. Ardissone, A.A. Lemonidou, E. Heracleous, E. López, M.N. Pedernera, D.O. Borio, Ind. Eng. Chem. Res. 48 (2009) 1090.
[19] E. Heracleous, A. Delimitis, L. Nalbandian, A.A. Lemonidou, Appl. Catal. A 325 (2007) 220.
[20] A.A. Lemonidou, Abstract 9th Novel Gas Conversion Symposium, Lyon, 2010, KN11, p. 36.
[21] B. Solsona, A. Dejoz, M.I. Vázquez, F. Ivars, J.M. López Nieto, Top. Catal. 52 (2009) 751.
[22] J.M. Quintana Melgoza, J. Cruz Reyes, M. Avalos-Borja, Mater. Lett. 47 (2001) 314–318.
[23] B. Scheffer, P. Molhoek, J.A. Moulijn, Appl. Catal. 46 (1989) 11.
[24] Ch. Li, Y.-W. Chen, Thermochim. Acta 256 (1995) 457–465.
[25] R. Fiuza, M.A. Silva, J.S. Boaventura, Int. J. Hydrogen Energy 35 (2010) 11216.
[26] A. Spojakina, R. Palcheva, K. Jiratova, G. Tyuliev, L. Petrov, Catal. Lett. 104 (2005) 45.
[27] Q. Zhao, Sh. Chen, J. Gao, Ch. Xu, Transition Met. Chem. 34 (2009) 621.
[28] M.J. Tomellini, J. Chem. Soc. Faraday Trans. 1 (84) (1988) 350.
[29] M.W. Roberts, R.J. Smart, J. Chem. Soc. Faraday Trans. 1 (80) (1984) 2957.
[30] P. Salagre, J.L.G. Fierro, F. Medina, J.E. Sueiras, J. Mol. Catal. A 106 (1996) 125.
[31] J.C. Vedrine, G. Hollinger, T.M. Duc, J. Phys. Chem. 82 (1978) 1515.
[32] M.A. van Veenendaal, G.A. Sawatzky, Phys. Rev. Lett. 70 (1993) 2459.
[33] V. Biju, M. Abdu Khadar, J. Nanopart. Res. 4 (2002) 247.
[34] M.A. van Veenendaal, D. Alders, G.A. Sawatzky, Phys. Rev. B 51 (1995) 13966.
[35] D. Alders, F.C. Voogt, T. Hibma, G.A. Sawatzky, Phys. Rev. B 54 (1996) 7716.
[36] E. Salje, A.F. Carley, M.W. Roberts, J. Solid State Chem. 29 (1979) 237.
[37] J. Haber, J. Stoch, L. Ungier, J. Solid State Chem. 19 (1976) 113.
[38] F. Hilbrig, H. Schmelz, H. Knözinger, in: L. Guzci, F. Solymosi, P. Tétényi (Eds.), Proceedings of the 10th International Congress on Catalysis, Elsevier, Amsterdam, 1993, p. 1351.
[39] G. Busca, V. Lorenzelli, V. Sánchez-Escribano, Chem. Mater. 4 (1992) 595.
[40] K. Hadjivanov, H. Knözinger, M. Mihaylov, J. Phys. Chem. B 106 (2002) 2618.
[41] J. Zhu, J.G. van Ommen, H.J.M. Bouwmeester, L. Lefferts, J. Catal. 233 (2005) 434.
[42] X. Zhang, Y. Gong, G. Yu, G.Y. Xie, J. Mol. Catal. A Chem. 180 (2002) 293.
[43] H. Fu, Z.-P. Liu, Z.-H. Li, W.-N. Wang, K.-N. Fan, J. Am. Chem. Soc. 128 (2006) 11114.